ChemComm

Accepted Manuscript

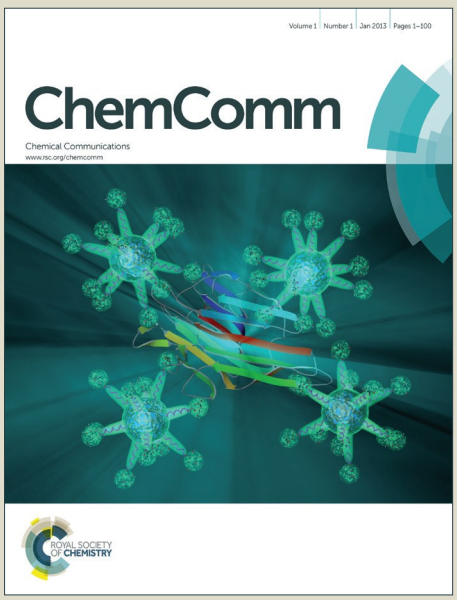

ROYAL SOCIETY OF CHEMISTRY

www.rsc.org/chemcomm

Journal Name

RSCPublishing

COMMUNICATION

Anatomy of Screw Dislocations in Nanoporous SAPO-18 as revealed by Atomic Force Microscopy

Cite this: DOI: 10.1039/x0xx00000x

Rachel L. Smith,[a] Anna Lind,[b] Duncan Akporiaye,[b] Martin P. Attfield,[a] and Michael W. Anderson[a,*]

Received 00th January 2012,
Accepted 00th January 2012

DOI: 10.1039/x0xx00000x

www.rsc.org/

Defects in solids are often the source of functional activity, the trigger for crystal growth and the seat of instability. Screw dislocations are notoriously difficult to study by electron microscopy. Here we decipher the complex anatomy of one such defect in the industrially important nanoporous catalyst SAPO-18 by atomic force microscopy.

For over thirty years transmission electron microscopy (TEM) has been widely used to investigate extended defects in various nanoporous systems. TEM allows direct imaging of a wide range of defect structures with very high resolution. One of the early examples of HRTEM (high-resolution TEM) of nanoporous materials was the observation of the porous framework of zeolite A.[1] Later, zeolite intergrowths were investigated and twinning and stacking faults were observed in the FAU/EMT,[2] MFI/MEL[3] and zeolite beta[4] intergrowth systems. However, observation of screw dislocations by TEM methods is extremely challenging. TEM relies on electron build-up of the long-range structure in order to give a high-resolution image. The structure at a screw dislocation is different to the bulk crystal only at the core where a significant amount of strain is stored. Therefore, it is difficult to image the screw dislocation even with the beam focussed down the zone axis of the dislocation, which may or may not be orthogonal to the crystal facet. Atomic Force Microscopy (AFM) overcomes this problem because the spiral growth hillock generated from the screw dislocation can be imaged directly on the crystal surface. Further, AFM can be performed in solution permitting *in-situ* studies of growth or dissolution at the screw dislocation. The first crystal-growth AFM investigation of a zeolite[5] was performed in 1996 and since then a wide range of nanoporous systems have been investigated. Screw dislocations in nanoporous materials are surprisingly common despite the relatively large Burgers vectors associated with these defects that might suggest a large amount of strain would be stored at the screw core. Theoretical calculations on the possible structure at the core of a screw dislocation in zeolite A shows how this crystal strain can be accommodated in these open-framework structures.[6] Our group has now observed spiral growth in a large number of varied nanoporous systems. The synthesis of silicoaluminophosphate SAPO-18 was first reported[7] in 1994 after the preparation of the aluminophosphate analogue, AlPO-18, in 1982.[8] Silicon incorporation into the structure gives SAPO-18 its Brønsted acidity and it is an important catalyst in the Methanol-to-Olefins (MTO) process, which has recently been commercialised.[9] Crystal-growth investigations are especially important for catalytically active materials as the presence of defects can have profound effects on the catalytic properties. Here, we present the first AFM observations of SAPO-18 and show that the growth is dominated by a particularly complex spiral-growth mechanism.

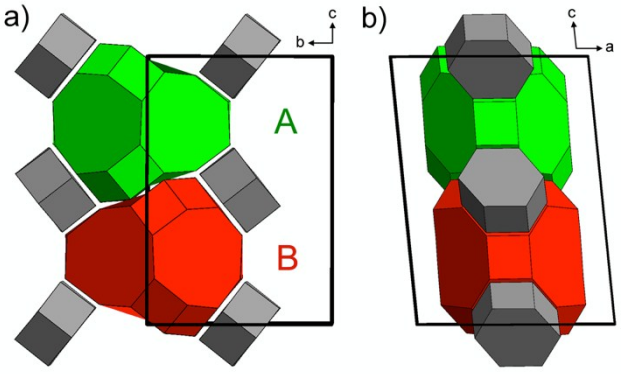

Figure 1. Cage structure and unit cell of SAPO-18 showing the double-6-rings (grey) and both orientations of the AEI-cage (red and green): a) viewed along the *a* direction; b) viewed along the *b* direction. The 'nose' of the AEI-cage is on the right in the A layer and the left in the B layer in (a).

SAPO-18 has the framework code **AEI** and the structure is given in Figure 1. Tilted double-6-rings (D6Rs, shown in grey) are connected by 4-membered rings to form the larger, pear-shaped cages (herein referred to as the AEI-cage – this is the same as the **per** polyhedra[10] or the **t-per** tile defined by Anurova *et al.*[11]). Owing to switching in the orientation of the D6Rs in the *c*-direction, the AEI-cages alternate orientation when stacking in the *c*-direction giving rise to both A and B layers (Figure 1a), where the 'nose' of the cage points in alternating directions. The unit cell dimensions were calculated from the powder pattern to give a = 13.493 Å, b = 12.619 Å, c = 18.413 Å and β = 95.33° (monoclinic space group *C2/c*). This unit cell is shown in Figure 1 in black and comprises both A and B layers. The 95° β angle is evident in Figure 1b.

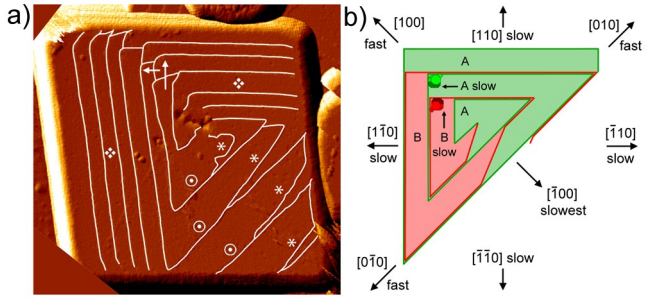

Figure 2. a) Vertical deflection atomic force microscopy image of the {001} face of SAPO-18 with the terrace edges outlined in white; b) schematic showing the basic structure of the screw dislocation and relative grow rates.

SAPO-18 crystals were successfully synthesised following the procedure outlined by Mertens *et al.*[9] Experimental details, X-ray diffraction patterns (Figure S1) and scanning electron microscopy images (Figure S2) can be found in the Supporting Information. The reaction was quenched at the end of the synthesis to avoid changes in supersaturation from slow cooling, as this may affect the features visible on the surface. The crystals were not calcined prior to AFM analysis and exhibited a typical square-platelet morphology.[12] Figure 2a shows an AFM image of a representative SAPO-18 crystal (additional AFM images are given in Figure S3). The terrace edges are outlined for clarity and the original, unlabelled image is available as Figure S4a. The surface of SAPO-18 displays a complex spiral growth pattern with interlaced terraces present on the top left of Figure 2a, with arrows showing interlaced steps of one layer height (i.e. an A or B layer, half the unit cell). At the lower right of the figure another step edge (indicated by ⊙) gives a triangular appearance to the spiral. The A and B layers emanate in concert from the screw core but then split (indicated by *) on the lower part of the figure. The heart of the dislocation near the core is characterised by small, ill-defined etch pits.

Terrace step heights were measured in order to determine the structure of the dislocation. The straight terraces (indicated by ❖ on Figure 2a) have step height 1.8 ± 0.1 nm (cross-section analysis is shown in Figure S4b). This corresponds to the unit-cell length in the *c*-direction of SAPO-18, demonstrating that the facet under investigation is the {001} face (as expected from the crystal habit). A schematic of the structure with crystallographic directions and relative growth rates is given in Figure 2b. These crystallographic directions were inferred from careful consideration of the AEI structure and relative growth rates. The [100] and [$\bar{1}$00] directions cannot be differentiated, and could be reversed, but these directions have been defined for clarity during the discussion. The step height across the interlaced terraces is 0.9 ± 0.1 nm, corresponding to a single A or B layer (half the unit cell, Figure S4c). The interlacing results from differences in growth rates between the A and B layer in the [110] and [1$\bar{1}$0] directions. This is due to the switch in orientation of the AEI-cage from layer A to layer B (Figure 1a). The AEI-cages are displayed on the interlaced terraces on Figure 2b. In a given direction, the 'nose' of the AEI-cage either points out on the edge of the step or back into the terrace. This leads to growth anisotropy between the layers and also in the two different directions. In Figure 2b the A layer is shown as growing quickly in the [110] direction, but it is possible that the A and the B layers should be switched as we cannot easily ascertain which permutation will be more stable. The upper, more stable layer grows out to stabilise the underlying layer. The two possible arrangements are shown as Figure 3a and Figure 3b.

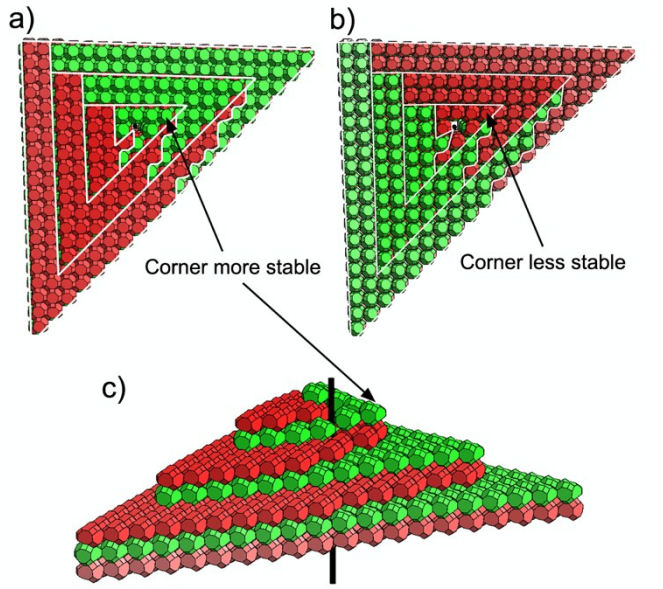

Figure 3. a) top-down view of the cage structure of the screw dislocation with terraces edges indicated by white lines; b) alternative structure where the order of A and B layers are reversed; c) oblique view of the structure shown in (a). The screw axis is given by the black line and D6Rs are omitted for clarity.

It has been shown in previous work[13] that the stable structures in a nanoporous framework material are the closed cages – in this case the AEI-cages and the double 6-rings. The closed cages at the surface of the crystal consist of a mixture of Q4 and Q3 tetrahedral sites. The stability of the cage is, to a first approximation, strongly related to the number of such sites, such that a cage with more Q3 sites will be less stable. However, in this case both permutations give four Q3 sites at the terrace edge (shown in Figure S5 in Supporting Information). The differentiation is that in one permutation the four Q3 sites are in an AEI cage and in the other permutation they are in a double 6-ring. Without a detailed

calculation of edge energy it is, therefore, not possible at this time to predict which of the two permutations is more stable.

The problem of edge stability, however, can be addressed by considering growth in the [$\bar{1}$00] direction. In the [$\bar{1}$00] direction (as it is defined in Figure 2b), interlacing does not occur because the growth rate is slower than the [$\bar{1}$10] and [$\bar{1}\bar{1}$0] directions and hence a new terrace edge is formed (shown in Figure 2a with ⊙). The growth rate along the *a*-direction is anisotropic because of the 95.33° tilt of the unit cell, which results in an acute and an obtuse edge. In calcite the obtuse step retreat upon dissolution is faster, thus the acute step is more stable.[14] It is possible that this is the same in the case of SAPO-18 but a detailed theoretical study would be required to determine which step is more stable. Splitting of the steps is visible on the AFM images (Figure 2a, shown by *) approximately half way along the terrace edge. These crystals are a record of the growth features near to equilibrium where there is a balance between growth and dissolution. Therefore, the splitting will be a consequence of this balance such that the terrace is dissolved until the dissolution is arrested and pinned at the corner (shown in Figure 3c) by the more stable corner in the layer above. We can determine which permutation is more stable by counting the number of Q3 sites in the cages at this corner and this reveals that the permutation shown in Figure 3a is more likely (Q3 count shown in Figure S6, Supporting Information). The acute angle that the split step adopts will also be a result of the balance between growth and dissolution such that the higher energy of the split step is countered by the shorter overall edge length (basic schematic given in Figure S7).

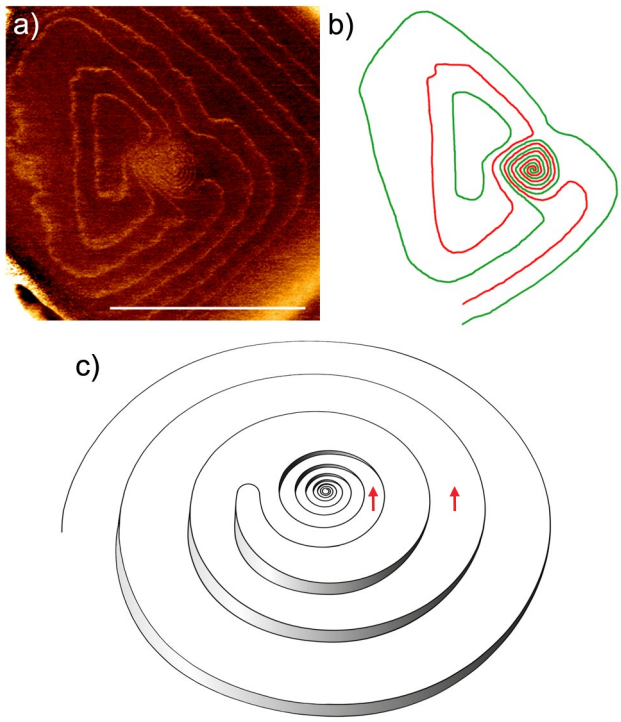

Figure 4. a) in-situ dissolution of SAPO-18 after 102 minutes in solution; b) schematic showing a trace of the terraces edges and the spiral dissolution pit on the dissolved crystal; c) 3D representation of a simple round spiral growth hillock with a spiral dissolution pit at its core. Red arrows show two terraces winding down from the same layer. Scale bar shown in a) is 500 nm.

The screw dislocation was examined further by dissolving the crystal in pH 5 H_3PO_4 solution and performing *in-situ* AFM. Figure 4a shows a SAPO-18 crystal after 102 minutes of dissolution where the surface has partly dissolved leading to separation of the terraces and loss of the interlaced structure. The most important feature is the increased size and internal structure of the etch pit at the centre of the dislocation. A spiral is visible running down into the crystal and a trace of the terrace pattern is given in Figure 4b. This is a spiral dissolution pit at the centre of the spiral growth hillock. A cross section across the surface is given in Figure S8 to show the height changes across the dislocation. A simplified schematic of the spiral is shown in Figure 4c and the red arrows show the direction that the terrace is winding down from the core (or into the core). Both arrows are shown on two terraces from the same layer, one inside the spiral dissolution pit and one outside on the main spiral growth hillock. The spiral maintains its handedness but it gives the appearance of the spiral changing direction.

Prior to dissolution, a small etch pit was apparent at the centre of the screw dislocation and these etch pits were universal to all crystals observed by AFM. *In-situ* AFM revealed that these etch pits are tight spiral dissolution pits. This is an unusual phenomenon and to our knowledge never reported previously. Interestingly, zeolite A crystals[15] showed similar etch pits but since these crystals were never investigated by *in-situ* methods it is unknown whether these are also spiral dissolution pits. Monte Carlo simulations show that during dissolution conditions spiral dissolution pits can be generated.[16] Many semiconductor materials show large holes at the centre of screw dislocations but are typically characterised as 'nanopipes' caused by open core screw dislocations.[17,18] In SiC, screw dislocations below three lattice constants do not have hollow cores but the ion-milled etch pits are smooth.[19]

The reason that a spiral dissolution pit is present at the centre of the dislocation is that, as discussed previously, these crystals are near equilibrium where there is a balance between growth and dissolution. As a consequence, the effect of dissolution at the screw core makes a small spiral dissolution pit of only *ca.* 50 nm and, therefore, cannot be properly imaged by the tip and appears as an ill-defined etch pit. When the feature being imaged is smaller than the size of the AFM tip then the tip is imaged rather than the surface features, resulting in an artefact being created. Upon further dissolution by acid the spiral dissolution pit expands from the core outwards making it accessible to the AFM tip. It is very unlikely that earlier in the synthesis, at higher supersaturation, that these spiral dissolution pits exist. It is much more likely that the spiral growth hillock would have a regular shape.

The SAPO-18 crystal shown in Figure 2a in fact has four adjacent screw dislocations of the same handedness, leading to a composite spiral pattern. A schematic of the structure is given in Figure 5a and the small spiral dissolution pits are shown (the spirals of the dissolution pits cannot be directly imaged by AFM but the structure is inferred from the pattern of the larger spiral dissolution pits visible after *in-situ* dissolution). Figure 5b shows an enlarged image of the spiral centre. The overall growth patterns are identical for a single dislocation or a composite dislocation as the same structural rules and relative growth rates apply. The cores of these

spiral dissolution pits have well-defined structure unlike any other materials currently reported in the literature.

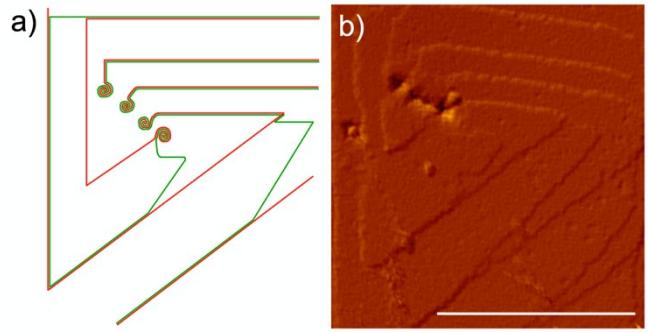

Figure 5. a) Schematic of the centre of the spiral for the crystal given in Figure 2a showing the small spiral dissolution pits at the core of the spiral growth hillock; b) enlarged AFM image of the centre of the screw dislocation. The terrace pattern is a result of a composite of four screw dislocations. The spiral dissolution pits can be seen as dark defects on the crystal surface. Scale bar shown on b) is 500 nm.

It is an important finding that the apparent ill-defined screw core is in fact a well-defined structure. Although we do not know the exact atomic structure at the screw core this result suggests that the structure is itself well defined. This is not surprising because of the facile manner in which these crystals grow via screw dislocations. It will be important in the future to perform both theoretical calculations and also careful electron microscopy studies in order to try to define exactly the atomic nature at these screw cores.

In conclusion, SAPO-18 crystal growth proceeds via a spiral growth mechanism with complex terrace patterns specific to the **AEI** structure. The unusual terrace pattern was fully described by consideration of the AEI-cage structure of the two layers in the SAPO-18 unit cell. However, there are still some uncertain elements such as the definitive arrangement of the A and B layers, the relative growth rates of the acute and obtuse steps, and the nature of the split terraces. Therefore, this structure would be amenable to detailed theoretical studies. These SAPO-18 screw dislocations are unique because at their core there was evidence of spiral dissolution pits. This gave the appearance of etch pits on the surface, but dissolution revealed the unusual spiral dissolution pit at the dislocation core. Understanding the crystal growth of nanoporous materials is the first step to control of the defect formation and thus the catalytic properties. Spiral growth is important when considering intergrowth formation because in many cases intergrowth cannot occur on a spiral growth hillock so the intergrowth is inhibited. This is particularly important in the industrially relevant CHA/AEI intergrowth system because spiral growth is an important growth mechanism in both SAPO-18 and SAPO-34 (**CHA**).[20] Therefore, these crystal growth observations have significant implications for defect incorporation in real industrial catalysts.

Notes and references

[a] Centre for Nanoporous Materials, School of Chemistry, The University of Manchester, Oxford Road, Manchester M13 9PL, UK.
[b] SINTEF Materials and Chemistry, P.O. Box 124, Blindern, 0314 Oslo, Norway.

Acknowledgements: This work is part of the InterCat Project (Intergrowth Materials for Improved Methanol-To-Olefin Catalysts) funded by the GASSMAX program of the Research Council of Norway, grant number 208325 and the EPSRC, UK. The authors would like to thank Tim Butler for the graphic in Figure 4c.

Electronic Supplementary Information (ESI) available: XRD and SEM data, supplementary AFM images, cross sectional analysis, Q3 site counts and experimental details. See DOI: 10.1039/c000000x/

1. L. A. Bursill, E. A. Lodge and J. M. Thomas, *Nature*, 1980, **286**, 111.
2. M. Audier, J. M. Thomas, J. Klinowski, D. A. Jefferson and L. A. Bursill, *J. Phys. Chem.*, 1982, **86**, 581.
3. G. R. Millward, S. Ramdas, J. M. Thomas and M. T. Barlow, *J. Chem. Soc., Faraday Trans. 2*, 1983, **79**, 1075.
4. J. M. Newsam, M. M. J. Treacy, W. T. Koetsier and C. B. De Gruyter, *Proc. R. Soc. Lond. A*, 1988, **420**, 375.
5. M. W. Anderson, J. R. Agger, J. T. Thornton and N. Forsyth, *Angew. Chem. Int. Ed. Engl.*, 1996, **35**, 1210.
6. A. M. Walker, B. Slater, J. D. Gale and K. Wright, *Nature Mater.,* 2004, **3**, 715.
7. J. Chen, J. M. Thomas, P. A. Wright and R. P. Townsend, *Catal. Lett.*, 1994, **28**, 241.
8. *US Pat.,* 4 310 440, 1982.
9. *WO Pat.,* 117 186, 2009.
10. W. H. Baur and R. X. Fischer, Microporous and other Framework Materials with Zeolite-Type Structures; Landolt-Börnstein New Series IV/14 Subvolume B: Zeolite Structure Codes ABW to CZP; Springer: Berlin, 2000.
11. N. A. Anurova, V. A. Blatov, G. D. Ilyushin and D. M. Proserpio, *J. Phys. Chem. C*, 2010, **114**, 10160.
12. R. Wendelbo, D. Akporiaye, A. Andersen, I. M. Dahl and H. B. Mostad, *Appl. Catal., A*, 1996, **142**, L197.
13. P. Cubillas, J. T. Gebbie, S. M. Stevens, N. Blake, A. Umemura, O. Terasaki and M. W. Anderson, *J. Phys. Chem. C,* 2014, **118**, 23092.
14. Y. Liang and D. R. Baer, *Surf. Sci.*, 1997, **373**, 275.
15. M. W. Anderson, J. R. Agger , L. I. Meza , C. B. Chong and C. S. Cundy, *Faraday Discuss.,* 2007, **136**, 143.
16. H. M. Cuppen, E. van Veenendaal, J. van Suchtelen, W. J. P. van Enckevort and E Vlieg, *J. Cryst. Growth*, 2000, **219**, 165.
17. W. Qian, G. S. Rohrer, M. Skowronski, K. Doverspike, L. B. Rowland and D. K. Gaskill, *Appl. Phys. Lett.,* 1995, **67**, 2284.
18. M. Grodzicki, P. Mazur, S. Zuber, G. Urbanik and A. Ciszewski, *Thin Solid Films*, 2008, **516**, 7530.
19 W. M. Vetter and M. Dudley, *J. Mater. Res.*, 2000, **15**, 1649.
20. B. Holme, P. Cubillas, J. H. Cavka, B. Slater, M. W. Anderson and D. Akporiaye, *Cryst. Growth. Des*., 2010, **10**, 2824.